International Journal of Innovative Computing, Information and Control
Volume **21**, Number **4**, August **2025**

ICIC International ©2025 ISSN 1349-4198
pp. **1119–1133**

MODEL PREDICTIVE CONTROL OF PV/BESS THREE-PHASE ELECTRIC SPRING IN MICROGRID

Zuhang Zhang[1], Tinglong Pan[1,*], Shunshun Ma[2], Jinlei Pei[1] and Dezhi Xu[2,3]

[1]School of Internet of Things Engineering
Jiangnan University
No. 1800, Lihu Avenue, Wuxi 214122, P. R. China
{ 6221915034; jlpei }@stu.jiangnan.edu.cn
*Corresponding author: tlpan@jiangnan.edu.cn

[2]School of Electrical Engineering
[3]Enginering Research Center of Electrical Transport Technology, Ministry of Education
Southeast University
No. 2, Sipailou, Xuanwu District, Nanjing 210096, P. R. China
{ 220225954; xudezhi }@seu.edu.cn

Received November 2024; revised March 2025

Abstract. *To address the impracticality of using an ideal DC source as the energy supply in traditional three-phase electric spring (TPES), this paper introduces a new topology, referred to as the photovoltaic and battery energy storage system TPES (PV/BESS TPES), which integrates a PV and BESS system to provide a stable DC power source. While this approach solves the energy supply issue and improves PV utilization, it also introduces additional disturbances, such as DC output voltage fluctuations caused by variations in solar irradiance, temperature, and grid voltage, which increase control complexity. To satisfy the high voltage quality requirements of critical loads (CLs), this paper adopts model predictive control (MPC) as the control strategy for the PV/BESS TPES, leveraging MPC's superior control accuracy in multivariable systems. Comparative analysis with traditional proportional-integral (PI) control demonstrates that MPC provides rapid response and effective adjustment under frequent multivariable fluctuations, thereby maintaining system stability and robustness.*

Keywords: Photovoltaic, Battery energy storage system, Three-phase electric spring, Critical load voltage, Model predictive control

1. **Introduction.** The growing integration of renewable energy sources, such as solar and wind power, into the electrical grid aims to address energy challenges and mitigate environmental impacts [1, 2]. However, the inherent variability and intermittency of these renewables can lead to significant fluctuations in voltage and frequency [3, 4]. During peak load periods, if renewable energy generation falls short of demand, the reliability of the power supply may be compromised. This situation poses significant risks for critical loads (CLs), such as medical equipment, military systems, and precision industrial facilities, which require stable and high-quality power to operate effectively. This variability places additional strain on grid stability. To address these challenges, the concept of the electric spring (ES) has emerged as a promising solution for enhancing power quality at the user level [5, 6, 7, 8]. ES operates by transferring voltage fluctuations from CLs to non-critical loads (NCLs) with more flexible power requirements, thereby stabilizing the power quality for CLs and supporting overall grid stability amidst renewable integration.

DOI: 10.24507/ijicic.21.04.1119

Initially, ES systems were primarily applied to stabilizing grid voltage and frequency. Subsequent research has expanded the use of ES systems through various circuit configurations to achieve more complex functions. Currently, there are three main types of ES systems: the original ES (ES-1) [9, 10, 11], the ES with an ideal voltage source (ES-2) [12], and the back-to-back ES (ES-b2b) [13]. ES-1 can directly provide reactive power compensation to NCLs while indirectly regulating their active power consumption. Building on ES-1, ES-2 incorporates a battery, enabling bidirectional active power flow and significantly expanding the operating range of the ES system. ES-B2B employs both parallel (grid-connected) and series (connecting the grid to NCLs) configurations. This dual configuration not only reduces battery-related costs associated with ES-2 but also further extends the operational capabilities of the ES system. Among these, ES-1 is the most extensively studied system due to its simple structure and effective control. Therefore, this paper focuses on the topology of the three-phase ES-1 (TPES-1) [14, 15, 16]. Extensive research has been conducted on power factor regulation and voltage stabilization strategies for TPES-1. In [17], a radial-chordal decomposition-based control method for TPES is introduced, allowing the energy storage system to provide active power compensation and mitigate three-phase power imbalances with minimal capacity requirements. [18] examines various voltage regulation functions and approaches for reducing power imbalances in TPES, based on instantaneous power theory. It further outlines conditions to minimize the average and oscillatory power of TPES and proposes different solutions. [19] implements a simple, easy-to-control proportional-integral (PI) controller with low interference for voltage and phase regulation in ES applications. However, in systems with multiple variables and strong nonlinearities, issues such as limited robustness and reduced regulation accuracy become more prominent.

Although existing research on TPES has demonstrated effective control performance, most studies assume an ideal voltage source as the power supply, yielding a constant DC output that is challenging to achieve in practical applications. To address this and improve PV utilization [20, 21, 22, 23, 24, 25, 26], this paper proposes a novel TPES topology that integrates a PV/BES into the design. While this approach addresses some limitations of previous models, it also introduces new challenges. Beyond managing grid voltage fluctuations, the system must account for variations in solar irradiance and temperature, which can impact DC output stability. Additionally, practical applications may encounter disturbances such as sudden load changes, posing risks to CLs that demand high-quality voltage. Under complex, multi-variable disturbances, traditional PI control methods often struggle to adjust TPES systems quickly when faced with frequent changes. In contrast, MPC [27, 28] provides a high-precision, low-energy control strategy suited for situations that require both accuracy and rapid response. MPC excels in multivariable, strongly coupled systems as it can manage multiple input and output variables simultaneously. By predicting system behavior based on a model, MPC anticipates and compensates for disturbances. When disruptions occur, MPC actively identifies and counteracts them, minimizing the impact of complex variables such as PV output fluctuations, grid instability, and temperature changes through real-time predictions and adjustments.

This paper thus proposes an MPC approach tailored for PV/BESS TPES systems to address the control challenges encountered in practical applications. The primary contributions and innovations are as follows.

1) In practical applications, the assumption of an ideal voltage source in traditional TPES configurations is impractical. To address this limitation, this study proposes an innovative topology integrating PV/BESS TPES. This advanced design not only resolves the energy supply challenges encountered in practical scenarios but also maximizes PV energy utilization, leading to significant improvements in overall system performance.

2) The control of PV/BESS TPES in practical applications presents considerable challenges due to fluctuations in both DC output voltage and grid voltage. These fluctuations are typically caused by factors such as variations in solar irradiance, temperature changes, and sudden load disturbances. To address these issues, this paper adopts MPC as the core control strategy, aiming to achieve precise regulation of CL voltage. The proposed MPC method, specifically designed for PV/BESS TPES, enables real-time prediction and dynamic adjustment of system behavior, ensuring optimal voltage control under multiple disturbances. By strictly adhering to system constraints, this approach significantly enhances the speed and stability of regulation, demonstrating exceptional adaptability and high performance in complex and dynamic real-world environments.

The remainder of this paper is structured as follows. Section 2 presents the design of the proposed controller for the PV/BESS TPES microgrid-connected system. Section 3 presents the control strategy, including the establishment of the PV/BESS system, the prediction of CL voltage, and the design of the cost function. Section 4 presents a comparison of the simulation and experimental results between MPC and PI control. Conclusions are provided in Section 5.

2. Working Principle of the PV/BESS TPES.

The traditional TPES system primarily consists of an ideal DC power source and a three-phase inverter. However, in practical applications, achieving a constant DC output is not feasible. Therefore, it is necessary to design a more suitable topology to enhance its applicability in real-world scenarios. Since ES systems are mainly used to address the fluctuations associated with renewable energy generation, integrating a PV/BESS system into the TPES can further improve the utilization of renewable energy. Figure 1 shows the controller structure of the PV/BESS TPES microgrid-connected system.

In the PV/BESS TPES, a three-phase inverter configuration is used, with the stable DC voltage connected to the inverter's DC link, and each inverter output is equipped with an

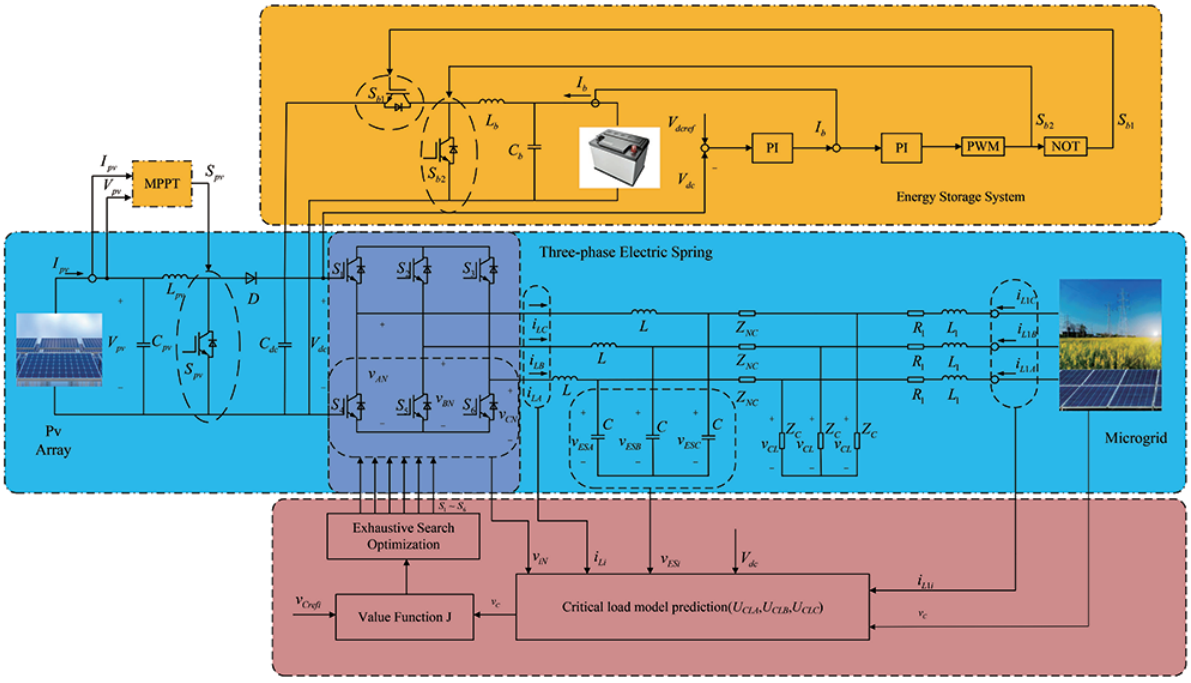

FIGURE 1. The structure of the proposed controller for PV/BESS TPES microgrid-connected system

LC filter. The energy supply for the PV/BESS TPES comes from the PV system, which utilizes maximum power point tracking (MPPT) to optimize solar energy capture and provide energy to the TPES. To address the uncertainty and variability of solar power generation, the BESS is connected in parallel with the PV system and linked through the PV system's capacitor terminals. This configuration stabilizes the DC output voltage by adjusting variations in solar irradiance and temperature through the charge and discharge cycles of the BESS.

The PV/BESS TPES is then connected in series with the NCL, forming a parallel intelligent load (SL) alongside the CL in the microgrid. When voltage fluctuations occur in the microgrid, the PV/BESS TPES adjusts the current supplied to the NCL, effectively transferring the voltage fluctuations from the microgrid side to the NCL. This mechanism ensures the stability of the CL voltage, enabling it to accurately track the reference value and maintain the required power quality.

3. **Model Predictive Control for the PV/BESS TPES.** Figure 1 illustrates the primary control strategy framework for the PV/BESS system, with MPC as its core, further detailed in Figure 2. Initially, the system measures the voltage and current of each phase, enabling the MPC model to predict the CL voltage under eight distinct switching states of the three-phase inverter. These predicted voltages are then compared to the reference values within the MPC cost function. By minimizing the cost function, the system identifies the optimal switching states for the six inverters. This strategy ensures that the CL voltage consistently tracks the reference, achieving robust and responsive voltage regulation across a wide range of operating conditions and external disturbances.

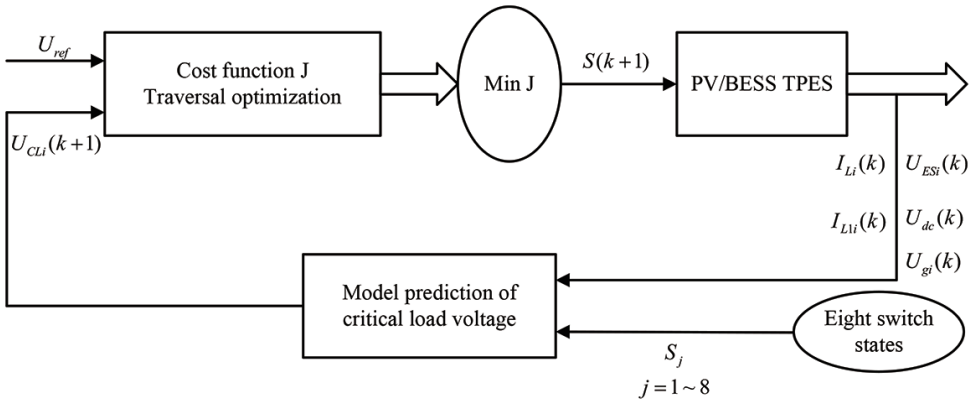

FIGURE 2. MPC control framework

3.1. **Control strategy of the PV/BESS system.** Compared to traditional TPES systems, the primary feature of the PV/BESS TPES is the use of solar energy as a power source. However, due to the characteristics of PV cells, the output power of the PV system is significantly influenced by factors such as solar irradiance and ambient temperature. To improve solar energy utilization and maximize the real-time power output of the PV system, maximum power point tracking (MPPT) control is essential.

To mitigate the impact of PV power fluctuations, BESS is utilized to stabilize bus voltage and suppress variations in PV power. The controllable switches S_{b1} and S_{b2} enable the converter to operate in two modes: boost and buck. In buck mode, S_{b2} is turned off. Conversely, the S_{b1} is turned off in boost mode. The circuit model for the buck mode can be expressed as

$$\begin{cases} L_b \dfrac{dI_b}{dt} = V_b,\ S_{b1} = 0,\ S_{b2} = 1 \\ L_b \dfrac{dI_b}{dt} = V_b - V_{DC},\ S_{b1} = 0,\ S_{b2} = 0 \end{cases} \tag{1}$$

The boost mode can be expressed as

$$\begin{cases} L_b \dfrac{dI_b}{dt} = V_{DC} - V_b,\ S_{b1} = 1,\ S_{b2} = 0 \\ L_b \dfrac{dI_b}{dt} = -V_b,\ S_{b1} = 0,\ S_{b2} = 0 \end{cases} \tag{2}$$

I_b and V_b denote the current passing through the inductor L_b and the voltage across the capacitor C_b within the PV system, respectively. Fluctuations in PV output due to environmental conditions can cause variations in V_{DC}. To tackle this issue, the BESS is employed, which stabilizes the bus voltage through a dual-loop control strategy. The outer voltage loop uses a PI controller to adjust the bus voltage error, providing a reference current for the inductor. The inner current loop controller regulates the inductor current and generates PWM control signals to manage the charge and discharge cycles of the BESS. This coordination between the BESS and the PV unit ensures a stable DC output, which serves as the energy source for the TPES.

3.2. **Prediction model for PV/BESS TPES.** The prediction model of the PV/BESS TPES serves as the foundation of the MPC framework, as it directly influences the accuracy of the control strategy. Achieving precise control begins with an analysis of the PV/BESS TPES topology, as depicted in Figure 1, where both the CL and NCL are modeled as purely resistive loads. By applying Kirchhoff's Current and Voltage Laws, the following equations are derived:

$$i_{NCi} = C\frac{dv_{ESi}}{dt} - i_{Li} \tag{3}$$

$$\frac{i_{NCi} + R_{NC}}{R_C} + i_{NCi} = i_{L1i} \tag{4}$$

$$L\frac{di_{Li}}{dt} + v_{ESi} = v_{iN} \tag{5}$$

$$L\frac{di_{Li}}{dt} + i_{L1i}R_1 + v_{ESi} + i_{NCi}R_{NC} = v_{Gi} \tag{6}$$

$$v_{Ci} = v_{ESi} + i_{NCi}R_{NC} \tag{7}$$

$$v_{Ci} = v_{Gi} + i_{L1i}R_1 - L_1\frac{di_{L1i}}{dt} \tag{8}$$

In the formulas, i represents any of the three phases – A, B, or C. v_{Gi} is the voltage of the microgrid for phase i, and v_{ESi} denotes the PV/BESS TPES voltage for phase i. i_{Li} represents the output filter inductance current of the PV/BESS TPES for phase i, while i_{L1i} represents the input current from the grid side for phase i. Additionally, v_{Ci} is the voltage of the CL and i_{NCi} is the current of NCL for phase i. L_1 denotes the equivalent inductance of the transmission line, while R_1 represents its equivalent resistance. Additionally, C and L correspond to the output filter capacitance and inductance of the PV/BESS TPES, respectively. The resistances of the CL and NCL are represented by R_C and R_{NC}.

It can be obtained by sorting through Formulas (3)-(6)

$$\begin{cases} \dfrac{di_{Li}}{dt} = -\dfrac{v_{ESi}}{L} + \dfrac{v_{iN}}{L} \\ \dfrac{dv_{ESi}}{dt} = \dfrac{i_{Li}}{C} - \dfrac{v_{ESi}}{C(R_C + R_{NC})} + \dfrac{R_C i_{L1i}}{C_i(R_C + R_{NC})} \\ \dfrac{di_{L1i}}{dt} = -\dfrac{R_C v_{ESi}}{L_1(R_C + R_{NC})} - \dfrac{(R_1R_C + R_1R_{NC} + R_CR_{NC})i_{L1i}}{L_1(R_C + R_{NC})} + \dfrac{v_{Gi}}{L_1} \end{cases} \tag{9}$$

where, v_{iN} represents the voltage of phase i at the inverter output relative to the neutral point.

By eliminating the NCL current i_{NCi} using Formulas (9) and (8), the following expression can be obtained

$$v_{Ci} = \frac{R_C}{R_C + R_{NC}} v_{ESi} + \frac{R_C R_{NC}}{R_C + R_{NC}} i_{L1i} \tag{10}$$

Applying the first-order forward difference method to Formula (9), the resulting expression can be obtained.

$$\begin{cases} i_{Li}(k+1) = i_{Li}(k) - \dfrac{T_S}{L} v_{ESi}(k+1) + \dfrac{T_S}{L} v_{iN} \\ v_{ESi}(k+1) = \dfrac{v_{ESi}(k)}{m_2 T_S} + \dfrac{i_{Li}(k)}{m_2 C} + \dfrac{T_S v_{iN}}{m_2 LC} + \dfrac{R_C i_{L1i}(k)}{m_2 C(R_C + R_{NC})} \\ i_{L1i}(k+1) = \dfrac{i_{L1i}(k)}{m_1 T_S} - \dfrac{R_C v_{ESi}(k+1)}{m_2 L_1(R_C + R_{NC})} + \dfrac{1}{m_1 L_1} v_{Gi}(k) \end{cases} \tag{11}$$

The determination method for the coefficients m_1 and m_2 is as follows

$$m_1 = \frac{1}{T_S} + \frac{(R_1R_C + R_1R_{NC} + R_CR_{NC})}{L_1(R_C + R_{NC})} \tag{12}$$

$$m_2 = \frac{1}{T_S} + \frac{1}{C(R_C + R_{NC})} + \frac{T_S}{LC} \tag{13}$$

Further simplification of formula (11) yields the following

$$v_{ESi}(k+1) = m_4 v_{ESi}(k) + m_5 i_{Li}(k) + m_6 v_{iN} + m_7 i_{L1i}(k) + m_8 v_{Gi}(k) \tag{14}$$

where,

$$\begin{cases} m_3 = 1 + \dfrac{R_C^2}{m_1 m_2 L_1 C (R_C + R_{NC})^2} \\ m_4 = \dfrac{1}{m_2 m_3 T_S} \\ m_5 = \dfrac{1}{m_2 m_3 C} \\ m_6 = \dfrac{T_S}{m_2 m_3 L_f C_f} \\ m_7 = \dfrac{1}{m_1 m_2 m_3 C T_S (R_C + R_{NC})} \\ m_8 = \dfrac{R_C}{m_1 m_2 m_3 L_1 C (R_C + R_{NC})} \end{cases} \tag{15}$$

Finally, by substituting the prediction models of v_{ESi} and i_{Li} into Formula (10), the CL voltage prediction model for PV/BESS TPES is obtained

$$v_{Ci}(k+1) = \frac{R_C}{R_{NC}+R_C} v_{ESi}(k+1) + \frac{R_{NC}R_C}{R_{NC}+R_C} i_{Li}(k+1) \tag{16}$$

3.3. **Value function and exhaustive search optimization.** In addition to the prediction model, another critical element of MPC is the cost function. The selection of the cost function is determined by the specific control objectives, which vary depending on the desired outcomes. This study focuses on controlling the voltage of the CL in the TPES system, and thus, the cost function is selected accordingly:

$$J = |v_{CA}(k+1) - v_{CAref}| + |v_{CB}(k+1) - v_{CBref}| + |v_{CC}(k+1) - v_{CCref}| \tag{17}$$

Since the inverter output voltages relative to the neutral point v_{AN}, v_{BN}, and v_{CN} vary with different PV/BESS TPES switching states, there are a total of eight possible switching states, each corresponding to a distinct value of the cost function. These switching states are defined as follows

$$\begin{aligned} S_A &= \begin{cases} 1@S_1 = 1 \& S_4 = 0 \\ 0@S_1 = 0 \& S_4 = 1 \end{cases} \\ S_B &= \begin{cases} 1@S_3 = 1 \& S_6 = 0 \\ 0@S_3 = 0 \& S_6 = 1 \end{cases} \\ S_C &= \begin{cases} 1@S_5 = 1 \& S_2 = 0 \\ 0@S_5 = 0 \& S_2 = 1 \end{cases} \end{aligned} \tag{18}$$

The corresponding three-phase neutral point voltages are obtained as follows

$$\begin{cases} v_{AN} = \dfrac{2V_{DC}}{3}(2S_A - S_B - S_C) \\ v_{BN} = \dfrac{2V_{DC}}{3}(2S_B - S_A - S_C) \\ v_{CN} = \dfrac{2V_{DC}}{3}(2S_C - S_B - S_A) \end{cases} \tag{19}$$

By substituting the CL voltage corresponding to the eight switching states into the value function, the optimal switching state is selected through the exhaustive search by minimizing the cost function. This approach allows for real-time tracking of the reference value for the CL voltage by controlling the PV/BESS TPES.

4. Simulation and Experimental Results.

4.1. **Analysis of simulation.** To validate the proposed method, a simulation was performed in the MATLAB/Simulink environment using the parameters listed in Table 1. Initially, to simulate PV operation, the illumination intensity is set to decrease continuously from 1000 Lux to 0 Lux between 0 and 0.4 seconds. V_{DCref} is set to 800 V. Additionally, the magnitude of the three-phase grid voltage is set to 311 V from 0 to 0.1 seconds, and the CL operates normally. To simulate the impact of PV and wind power generation on the microgrid voltage, the voltage magnitude is reduced to 270 V from 0.1 to 0.3 seconds and then increased to 320 V from 0.3 to 0.4 seconds. The PV/BESS TPES is connected at 0.2 seconds to regulate the voltage of the CL.

The controlled PV/BESS system maintains a relatively stable DC bus voltage despite external environmental changes, as shown in Figure 3. This configuration effectively meets the energy requirements of the TPES, ensuring reliable operation.

TABLE 1. Parameters for simulation

Parameters	Values
Microgrid frequency (f)	50 Hz
Microgrid voltage (v_G)	311 V
Line impedance (Z_1)	0.1 + 0.0024j Ω
Critical load resistance (R_C)	43.5 Ω
Non-critical load resistance (R_{NC})	2.2 Ω
Filter inductance (L)	0.003 H
Filter capacitance (C)	50 μF
Battery resistance (R_b)	0.1 Ω
Inductance of battery (L_b)	5 mH
Capacitance of the battery (C_b)	1 μF
PV inductance (L_{pv})	6 mH
PV capacitance (C_{pv})	0.01 F
DC bus capacitance (C_{DC})	0.02 F
Sampling time (T_s)	1×10^{-6} s

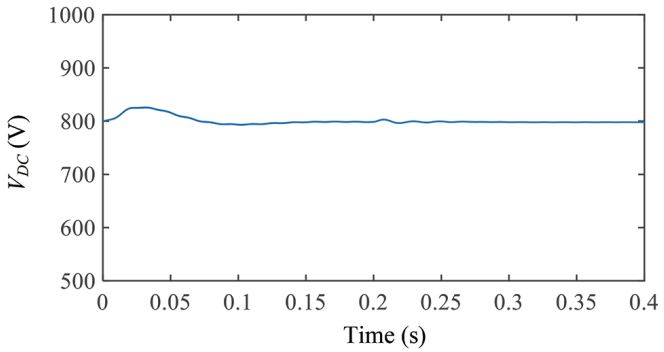

FIGURE 3. DC bus voltage

Under the simulation conditions described above, the PV/BESS TPES is controlled using both MPC and PI control, with the resulting performance shown below.

The voltage regulation of the CL under multiple disturbances, using both MPC and PI control, is shown in Figure 4. Initially, when the PV/BESS TPES system is not connected,

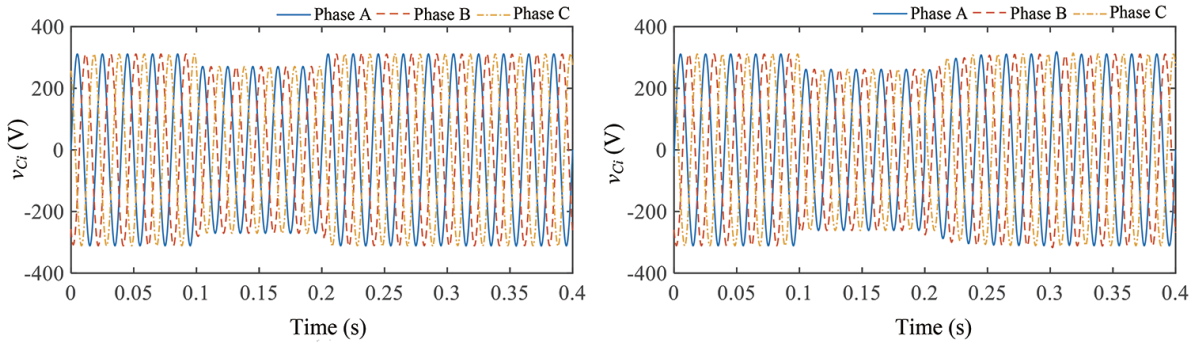

FIGURE 4. (a) CL voltage in MPC and (b) CL voltage in PI

the microgrid voltage remains stable at 311 V between 0 and 0.1 seconds, allowing the CL voltage to operate normally. However, between 0.1 and 0.2 seconds, the microgrid voltage decreases to 280 V, causing the CL voltage to drop below the reference value. At this point, the PV/BESS TPES system is connected, and the CL voltage begins to recover, eventually stabilizing at the reference value.

The root mean square (RMS) of voltage is a measure of the effective value of a varying voltage signal, commonly used in alternating current (AC) systems to represent the equivalent power that would be delivered by a direct current (DC) voltage. It is calculated by squaring all the voltage values, averaging them, and then taking the square root of that average. Figure 5(a) illustrates the RMS of the CL voltage under MPC control, where the voltage stabilizes rapidly at 220 V around 0.245 seconds. In contrast, Figure 5(b) shows the RMS value of the CL voltage under PI control, where it takes until approximately 0.27 seconds to return to the reference value. Furthermore, after validating the system's performance under low grid voltage conditions, the system was tested under high grid voltage, where the microgrid voltage was adjusted to 320 V between 0.3 and 0.4 seconds. Comparing the two control strategies, the results demonstrate that MPC control effectively maintains the stability of the CL voltage, while PI control experiences oscillations before stabilizing. This clearly illustrates the superior performance of MPC in handling grid voltage fluctuations and achieving rapid recovery, ensuring faster and more precise CL voltage regulation, and maintaining system stability and reliability under varying operating conditions.

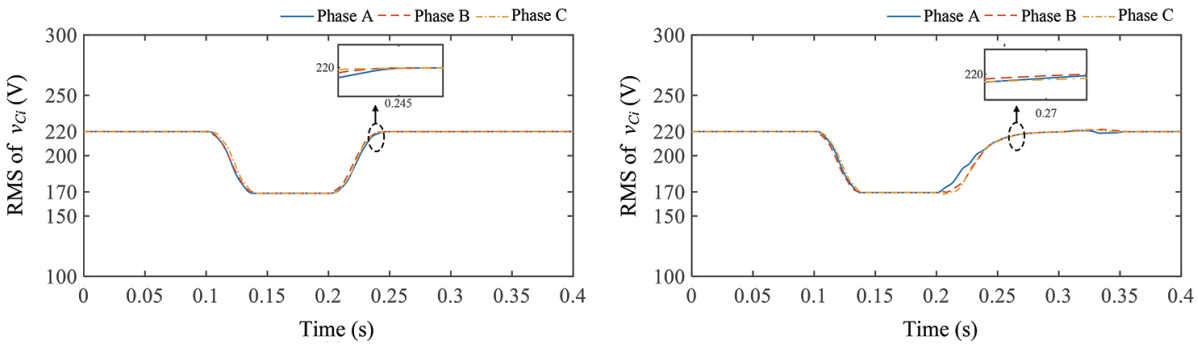

FIGURE 5. (a) RMS of CL voltage in MPC and (b) RMS of CL voltage in PI

Total harmonic distortion (THD) quantifies the distortion in a signal caused by the presence of harmonics, which are integer multiples of the signal's fundamental frequency. It is calculated by comparing the sum of the powers of all harmonic frequencies to the power of the fundamental frequency, typically expressed as a percentage. THD provides a measure of the harmonic distortion within a signal, indicating how much it deviates from its ideal, pure form. A higher THD value suggests greater distortion and lower signal quality, which can negatively impact the performance of electrical systems, such as power grids, audio systems, and electronic devices. Figure 6 compares the THD of V_C after stabilization using two different control algorithms. Under PI control, the harmonic distortion rate of v_{Ci} is 0.61% with an amplitude of 308.8 V. In contrast, under MPC control, the harmonic distortion rate of v_{Ci} is reduced to 0.29% with an amplitude of 310 V. This indicates that the voltage quality is significantly higher under MPC control.

In conclusion, under multiple disturbances, the PV/BESS TPES system demonstrates significantly superior speed and stability when controlled by MPC compared to PI control.

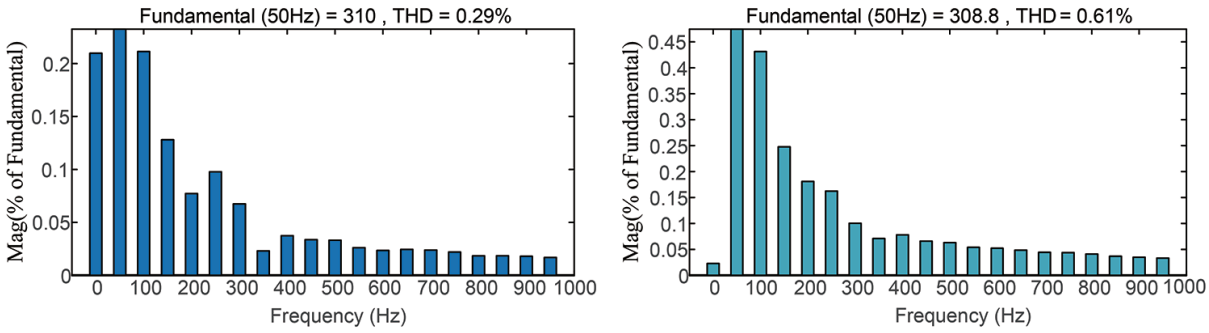

(a) (b)

FIGURE 6. (a) THD of CL voltage in MPC and (b) THD of CL voltage in PI

4.2. **Experimental results.** The proposed control strategy for the Distributed PV/BESS TPES has been realized through a hardware-in-the-loop (HIL) testing environment. This setup is depicted in Figure 7. Specifically, the circuit topology of the PV/BESS TPES energy system is established and then compiled on the HIL real-time simulator MT 3200. This simulator transmits voltage, current, and power signals to the proposed controller implemented in dSPACE 1202 and receives PWM signals to complete the closed-loop control process. Both hardware components are connected to the host computer via TCP/IP.

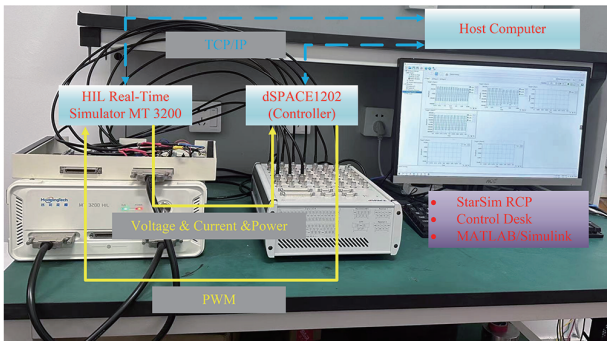

FIGURE 7. HIL experimental platform

An experimental platform was established to construct a PV/BESS TPES model with parameters identical to those used in the simulation. Under the same multi-disturbance conditions, by controlling the charge and discharge of the PV/BESS system, the system quickly returns to the bus voltage reference value when subjected to external disturbances, as shown in Figure 8. The output voltage V_{DC} is stabilized around 800 V, providing a stable energy source for the TPES. This demonstrates the reliability of the PV/BESS system in the experiment.

In the experimental setup, the PV/BESS TPES is integrated into the system at 0.2 seconds. Initially, from 0 to 0.1 seconds, the CL operates under nominal conditions. However, between 0.1 and 0.2 seconds, the grid voltage experiences a sudden drop to 280 V. Since the PV/BESS TPES has not yet been activated during this period, it is unable to mitigate the voltage fluctuation. At 0.2 seconds, once the PV/BESS TPES is connected, voltage fluctuations induced by sudden changes in grid voltage are dynamically redistributed to the NCL through MPC, as illustrated in Figure 9. The results presented in Figure 10 further demonstrate that immediately upon activation, the CL voltage rapidly recovers from the low-voltage state to its reference value of 311 V. Furthermore, when the

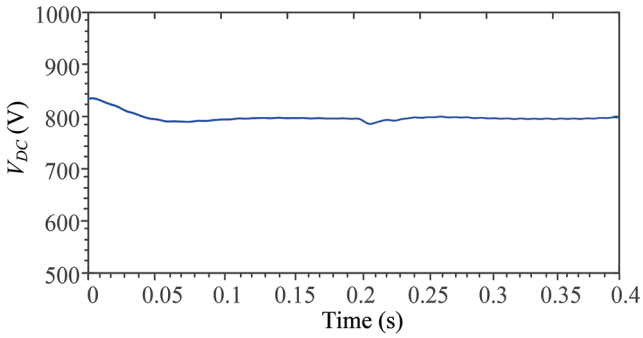

FIGURE 8. The DC bus voltage in the experiment

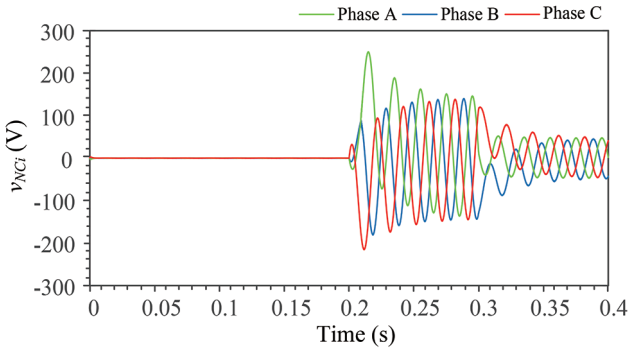

FIGURE 9. (color online) NCL voltage in MPC

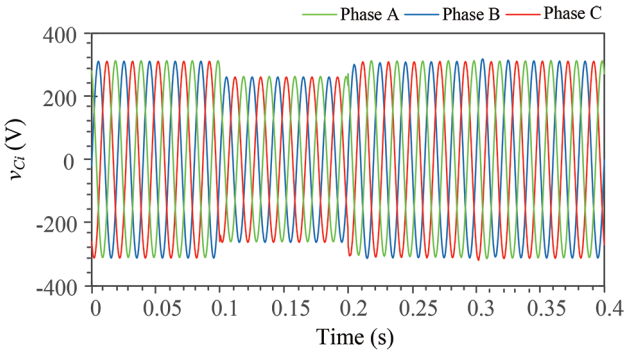

FIGURE 10. (color online) CL voltage in MPC

grid voltage abruptly rises to 320 V at 0.3 seconds, the CL voltage remains stable, accurately tracking the reference voltage in real time. These results highlight the effectiveness of the PV/BESS TPES in ensuring voltage stability and its ability to provide a rapid and robust response under dynamic grid conditions.

5. **Conclusion and Future Work.** This paper proposes an innovative TPES topology, termed the PV/BESS TPES, which replaces the ideal voltage source that is unfeasible in practical applications with a PV/BESS configuration to maximize PV energy utilization. In the presence of various disturbances, MPC effectively maintains the CL voltage close to the reference level, demonstrating robustness under dynamic conditions. Comparative simulations between MPC and traditional PI control reveal that MPC offers significant advantages in response speed and stability, particularly in environments characterized by external fluctuations and variable inputs. Furthermore, experimental results validate

the system's stability and reliability under MPC control, confirming that the PV/BESS TPES not only operates stably in practical settings but also significantly enhances voltage quality and resilience. These findings underscore the effectiveness of the PV/BESS TPES and highlight its potential for broader application in renewable-integrated power grids.

The topology and control strategies of TPESs have been extensively studied, demonstrating effective control performance. However, a single TPES can only ensure voltage stability for CL within a limited range of grid voltage fluctuations. This restricted control range constrains its further development and practical application. Future research could explore the parallel operation of multiple TPESs and optimize control algorithms to address potential challenges such as circulating currents. By enhancing coordination and stability in parallel operation, these advancements would significantly improve the control capability of TPESs and expand their applicability in real-world power systems.

Acknowledgment. This work is partially supported by the National Natural Science Foundation of China (Grant No. 62222307, No. 61973140) and the Natural Science Foundation of Jiangsu Province (Grant No. BK20211235). The authors also appreciatively acknowledge the helpful suggestions and comments of the reviewers, which have enhanced the presentation.

REFERENCES

[1] T. Kerekes, R. Teodorescu, M. Liserre, C. Klumpner and M. Sumner, Evaluation of three-phase transformerless photovoltaic inverter topologies, *IEEE Transactions on Power Electronics*, vol.24, no.9, pp.2202-2211, 2009.

[2] Y. Karimi, H. Oraee, M. S. Golsorkhi and J. M. Guerrero, Decentralized method for load sharing and power management in a PV/battery hybrid source islanded microgrid, *IEEE Transactions on Power Electronics*, vol.32, no.5, pp.3525-3535, 2017.

[3] F. Blaabjerg, Z. Chen and S. B. Kjaer, Power electronics as efficient interface in dispersed power generation systems, *IEEE Transactions on Power Electronics*, vol.19, no.5, pp.1184-1194, 2004.

[4] H. Yang, T. Li, Y. Long and Y. Xiao, Event-triggered distributed secondary control with model-free predictive compensation in ac/dc networked microgrids under DoS attacks, *IEEE Transactions on Cybernetics*, vol.54, no.1, pp.298-307, 2022.

[5] W. He, D. Qiu, B. Zhang, Y. Chen, F. Xie and W. Xiao, Extending the operation range of electric spring with dual inverters, *IEEE Transactions on Power Electronics*, 2023.

[6] A. Andreotti, B. Caiazzo, E. Fridman, A. Petrillo and S. Santini, Distributed dynamic event-triggered control for voltage recovery in islanded microgrids by using artificial delays, *IEEE Transactions on Cybernetics*, 2024.

[7] Q. Fu, L. F. Montoya, A. Solanki, A. Nasiri, V. Bhavaraju, T. Abdallah and C. Y. David, Microgrid generation capacity design with renewables and energy storage addressing power quality and surety, *IEEE Transactions on Smart Grid*, vol.3, no.4, pp.2019-2027, 2012.

[8] D. Qiu, C. Yuan, B. Zhang, M. Ke, Y. Chen and F. Xie, An improved electric spring topology based on LCL filter, *IEEE Transactions on Power Electronics*, vol.37, no.5, pp.5984-5994, 2022.

[9] C. K. Lee, B. Chaudhuri and S. Y. Hui, Hardware and control implementation of electric springs for stabilizing future smart grid with intermittent renewable energy sources, *IEEE Journal of Emerging and Selected Topics in Power Electronics*, vol.1, no.1, pp.18-27, 2013.

[10] X. Luo, J. Wang, M. Dooner and J. Clarke, Overview of current development in electrical energy storage technologies and the application potential in power system operation, *Applied Energy*, vol.137, pp.511-536, 2015.

[11] Q. Wang, M. Cheng, Z. Chen and Z. Wang, Steady-state analysis of electric springs with a novel δ control, *IEEE Transactions on Power Electronics*, vol.30, no.12, pp.7159-7169, 2015.

[12] S.-C. Tan, C. K. Lee and S. Y. Hui, General steady-state analysis and control principle of electric springs with active and reactive power compensations, *IEEE Transactions on Power Electronics*, vol.28, no.8, pp.3958-3969, 2013.

[13] Z. Akhtar, B. Chaudhuri and S. Y. R. Hui, Smart loads for voltage control in distribution networks, *IEEE Transactions on Smart Grid*, vol.8, no.2, pp.937-946, 2015.

[14] S. Yan, S.-C. Tan, C.-K. Lee, B. Chaudhuri and S. Y. R. Hui, Electric springs for reducing power imbalance in three-phase power systems, *IEEE Transactions on Power Electronics*, vol.30, no.7, pp.3601-3609, 2015.

[15] H. Liu, W. M. Ng, C.-K. Lee and S. Y. R. Hui, Integration of flexible loads and electric spring using a three-phase inverter, *IEEE Transactions on Power Electronics*, vol.35, no.8, pp.8013-8024, 2020.

[16] S. Mohanty, S. Pati, S. K. Kar, H. Kraiem, A. Flah, C. Z. El-Bayeh and M. Alqarni, A novel electric spring with improved range of operation for isolated microgrid systems, *IEEE Access*, 2023.

[17] K.-T. Mok, S.-S. Ho, S.-C. Tan and S. Y. Hui, A comprehensive analysis and control strategy for nullifying negative- and zero-sequence currents in an unbalanced three-phase power system using electric springs, *IEEE Transactions on Power Electronics*, vol.32, no.10, pp.7635-7650, 2017.

[18] S. Yan, M.-H. Wang, T.-B. Yang, S.-C. Tan, B. Chaudhuri and S. Y. R. Hui, Achieving multiple functions of three-phase electric springs in unbalanced three-phase power systems using the instantaneous power theory, *IEEE Transactions on Power Electronics*, vol.33, no.7, pp.5784-5795, 2018.

[19] Q. Wang, M. Cheng, Y. Jiang, W. Zuo and G. Buja, A simple active and reactive power control for applications of single-phase electric springs, *IEEE Transactions on Industrial Electronics*, vol.65, no.8, pp.6291-6300, 2018.

[20] D. Xu, J. Liu, X.-G. Yan and W. Yan, A novel adaptive neural network constrained control for a multi-area interconnected power system with hybrid energy storage, *IEEE Transactions on Industrial Electronics*, vol.65, no.8, pp.6625-6634, 2018.

[21] D. Xu, W. Zhang, B. Jiang, P. Shi and S. Wang, Directed-graph-observer-based model-free cooperative sliding mode control for distributed energy storage systems in dc microgrid, *IEEE Transactions on Industrial Informatics*, vol.16, no.2, pp.1224-1235, 2019.

[22] Y. Hong, D. Xu, W. Yang, B. Jiang and X.-G. Yan, A novel multi-agent model-free control for state-of-charge balancing between distributed battery energy storage systems, *IEEE Transactions on Emerging Topics in Computational Intelligence*, vol.5, no.4, pp.679-688, 2020.

[23] T. Yang, K.-T. Mok, S.-S. Ho, S.-C. Tan, C.-K. Lee and R. S. Y. Hui, Use of integrated photovoltaic-electric spring system as a power balancer in power distribution networks, *IEEE Transactions on Power Electronics*, vol.34, no.6, pp.5312-5324, 2019.

[24] Q. Liu, D. Xu, B. Jiang and Y. Ren, Prescribed-performance-based adaptive control for hybrid energy storage systems of battery and supercapacitor in electric vehicles, *International Journal of Innovative Computing, Information and Control*, vol.16, no.2, pp.571-583, 2020.

[25] T. Zhang, Q. Hao, Z. Zheng and C. Lu, An electric spring control strategy based on finite control set-model predictive control, *Journal Européen des Systèmes Automatisés*, vol.53, no.4, 2020.

[26] Q. Wang, D. Zha, M. Cheng, F. Deng and G. Buja, Energy management system for dc electric spring with parallel topology, *IEEE Transactions on Industry Applications*, vol.56, no.5, pp.5385-5395, 2020.

[27] W. Yang, C. Zhao, G. Hu, D. Xu and T. Pan, Hierarchical distributed model predictive control for multiple hybrid energy storage systems in a dc microgrid, *International Journal of Innovative Computing, Information and Control*, vol.19, no.6, pp.1735-1751, 2023.

[28] J. Rodrıguez, J. Pontt, C. Silva, M. Salgado, S. Rees, U. Ammann, P. Lezana, R. Huerta and P. Cortés, Predictive control of three-phase inverter, *Electron. Lett.*, vol.40, no.9, pp.561-562, 2004.

Author Biography

Zuhang Zhang received his B.Eng. degree in Electrical Engineering and Automation from Anhui University of Science and Technology, in 2022. At present, he is currently working toward the M.S. degree in Electrical Engineering at Jiangnan University.

His research interests include electric spring, model predictive control and multi agent.

Tinglong Pan received his B.Eng. degree in Industrial Automation from China University of Mining and Technology, Xuzhou, China, in 1999, and the Ph.D. degree in Power Electronics and Power Drive from China University of Mining and Technology, Xuzhou, China, in 2004.

He is currently a Professor at Jiangnan University, where his research interests include microgrid control technology, power conversion technology, power drive system and its intelligent control technology.

Shunshun Ma received his B.Eng. degree in Electrical Engineering and Automation from Jiangnan University in 2022. He is currently pursuing an M.S. degree in Electronic Information at Southeast University.

His research interests include image recognition, modeling of magnetic components, and the application of artificial intelligence in electrical engineering.

Jinlei Pei received the B.S. degree in Electrical Engineering and Automation from Hainan University, Haikou, China in 2018. He is currently working toward the Ph.D. degree in Control Engineering with Jiangnan University, Wuxi, China.

His current research interests include fault diagnosis and fault-tolerant control, multi-agent systems and smart grid.

Dezhi Xu received the Ph.D. degree in Control Theory and Control Engineering from Nanjing University of Aeronautics and Astronautics, China, in 2013.

From 2018 to 2019, he was a Visiting Fellow with the Department of Biomedical Engineering, City University of Hong Kong, Hong Kong. He is currently a Professor with a Young Endowed Chair Honor with the School of Electrical Engineering, Southeast University, Nanjing, China. His research interests include data-driven control, fault diagnosis and fault-tolerant control, multiagent systems and cyber-physical systems, technologies of renewable energy, motor control, and smart grid. He was a Guest Editor for the International Journal of Innovative Computing, Information and Control and the Electric Power. He is a Committee Member of the Association of Energy Internet, and Trusted Control in Chinese Association of Automation (CAA), and the Energy Storage in China Renewable Energy Society (CRES). He was supported by the National Natural Science Fund for Excellent Young Scientists Fund Program in 2022.